Sustainable Cities and Society 76 (2022) 103465

Contents lists available at ScienceDirect

Sustainable Cities and Society

journal homepage: www.elsevier.com/locate/scs

Energy burden and air conditioning adoption in New York City under a warming climate

L. Ortiz [a,*], H. Gamarro [b], J.E. Gonzalez [b], T. McPhearson [a,c,d]

[a] Urban Systems Lab, The New School, New York, NY, US
[b] Mechanical Engineering Department, The City College of New York, New York, NY, US
[c] Cary Institute of of Ecosystem Studies, Millbrook, NY, US
[d] Stockholm Resilience Centre, Stockholm, SE

ARTICLE INFO

Keywords:
Urban climate
Heat risk
Energy burden
Urban heat island

ABSTRACT

Global climate change has increased the need for cooling indoor spaces, leading to a rise in adoption of air conditioning. This adoption, while decreasing health risks, can increase energy use and pose economic burdens in low income households. Here, we estimate the burden associated with cooling, as well as potential extreme heat exposure without it in the largest city in the US, New York using a coupled weather and building energy model, utility pay scales, and household income data from the US Census.Results show uneven distribution of AC economic burden, with lower income neighborhoods experiencing the largest relative costs. High-burden neighborhoods see the largest climate-driven increases in spite of lower enthalpy increases. These neighborhoods also have the most exposure to indoor extreme heat, which may triple by end of century. Energy burden may pose a barrier to AC operation, with estimated cost in the lowest income households reaching up to 6.1% of income for a 100 m^2 dwelling, which could increase to 8% by end of century. We also explore adaptation strategies and quantify their impacts, finding that modifying traditional set points and reflective roofs can reduce energy burden significantly, by up to 20% in the highest burden neighborhoods.

1. Introduction

As temperatures continue to rise due to global climate change, so is the frequency and intensity of hazardous heat (Meehl and Tebaldi 2004). This increase in summer heat places unique challenges in cities, where population and infrastructure density may lead to higher mortality (Limaye et al. 2018) and critical systems failure (Chester et al. 2020). These increasing risks necessitate the use of adaptations to cool not only outdoor, but also indoor spaces. The most common indoor cooling in the US adaptation is air conditioning (AC). Although an effective tool to lower heat-related risks, AC adoption increases energy use while, with higher sensitivity in cities, where the majority of the global population resides (Waite et al. 2017), which may pose a significant challenge to sustainability goals focused being implemented in cities. Costs associated with this increased energy use may burden households unevenly, with low-income homes potentially being unable to prevent hazardous indoor heat.

1.1. Cooling cities in a changing climate

With global air temperatures projected to rise significantly, AC adoption is also projected to increase. In the US, the number of households with AC has increased from 66.1 million in 1993 to over 100 million in 2015, representing an adoption rate change from 66.1% to 87% (Energy Information Agency 2015). Meanwhile, the International Energy Agency (IEA) projects global AC ownership to soar to two thirds of all households by 2050 (International Energy Agency 2018). This increase in adoption, coupled with longer and warmer cooling seasons, has led to projected increases between 320% (low development scenario) to 2270% (high development scenario) in global residential cooling energy demand (Santamouris 2016). These upcoming changes present challenges at various scales, from regional and city scale power generation to accommodate the additional electric demand for space cooling, to utility costs at the household level.

This growing need for space cooling may be exacerbated in cities, where ambient temperatures are often higher than in surrounding areas. This phenomenon, called the Urban Heat Island (UHI), forms due to

* Corresponding author at: 79 Fifth Ave. 1604, New York, NY 10003
E-mail address: luis.ortiz.uriarte@gmail.com (L. Ortiz).

https://doi.org/10.1016/j.scs.2021.103465
Received 26 February 2021; Received in revised form 23 September 2021; Accepted 14 October 2021
Available online 29 October 2021

traditional built structures limiting cooling at the land surface (e.g., evaporative and radiative cooling), while both storing and generating more heat (e.g., AC use, traffic) (Oke 1982) than natural landscapes. Studies also show that UHIs may intensify periods of extreme heat locally due to the positive land-atmosphere feedbacks that lead to the UHI in the first place (Li and Bou-Zeid 2013; Founda and Santamouris 2017; Ramamurthy et al., 2017; Ortiz et al. 2018b; Ao et al. 2019). Moreover, the United Nations projects that urban areas will absorb most population growth projected by 2050 (United Nations 2019), further increasing health risks and cooling costs associated with summer heat.

When including both urban and climate signals, projections of cooling energy demand in New York City (NYC), the largest city in the US, show end of century increases of up to 80% in the business as usual RCP8.5 scenario (Ortiz et al. 2018a). Projected increases exhibited geospatial variation due to differences in built environment configuration and meteorological processes across the city such as sea breeze penetration. Geographic differences in near surface temperature increases mean that costs related to AC use will increase differently throughout the city, with varying consequences across groups with variable capacity to bear increased costs. Long-term summer climate projections in NYC have shown that although water vapor content of the atmosphere is expected to increase, relative humidity might slightly decrease (Ortiz et al. 2019), suggesting that increases in electric load might be driven by temperature increases rather than moisture content. In addition, building energy usage is affected by user behavior and equipment installation and repair. These factors cause disparities between energy ratings and actual usage, often called a performance gap, and may also lead to hard-to-quantify cooling costs (Sunikka-Blank and Galvin 2012; Calì et al. 2016). The performance gap may also be associated with socioeconomic factors (Palma et al. 2019), which can lead to already vulnerable populations being unevenly impacted by either high heat exposure or high costs of cooling.

1.2. Energy costs and burden

Study of energy costs as they relate to household income and poverty has often focused on heating during the cold season (Bhattacharya et al. 2003; Roberts 2008; Hills 2012; Teller-Elsberg et al. 2016; Robinson et al. 2018). However, year-round temperatures are expected to increase (Coumou et al. 2013; Lehner et al. 2018) for growing portions of the world (Coumou and Robinson 2013), likewise increasing the need and cost of AC operation while decreasing the need for heat (Wang and Chen 2014). The 2019 New York City Panel on Climate Change (NPCC) reported that while since 1900 there are on average 1.85 fewer days below freezing per decade, summer heat waves are expected to become more frequent, longer, and more intense (González et al. 2019). In NYC, premature mortality associated with warming summers is projected to grow between 47% to 95% by mid-century (Knowlton et al. 2007). Studies have also shown that low-income and minority groups in citires are often more vulnerable to heat (Hamstead et al. 2018; Madrigano et al. 2015b) and bear a higher energy cost burden, attributed mostly to differences in building infrastructure and investment (Kontokosta et al. 2019).

This disparity in relative energy costs may play a role in adoption of AC units in NYC, as reported by Ito et al (2018), who also found that areas with lower AC adoption coincide with higher rates of heat-related mortality and hospitalizations. Heat-related mortality and other health impacts are known to affect lower income and vulnerable populations like the elderly (Rosenthal et al. 2014) at higher rates. Although state and local governments sometimes provide economic assistance for heating and cooling, such as with the Home Energy Assistance Program (HEAP), these initiatives often only offer assistance in upfront costs, leaving residents to bear the cost burden of AC operation. Recent work focusing on Paris, France has also shown that while existing heat adaptation strategies (e.g., urban parks and white roofs) may partially offset heat risk and cooling loads, they are insufficient to completely eliminate projected increases, making AC an important tool to maintain thermal comfort and reduce heat-related illnesses (Viguie et al. 2020).

1.3. Modeling building energy demand at urban scales

One way to quantify household energy expenditures and their sensitivity to climate is by use of building energy models. Building energy models typically fall between two umbrellas: physics and statistical models. Physics-based models use energy and mass balance relationships information to quantify energy inputs and outputs to building envelopes. These models are often designed to resolve single buildings in high detail, as in the case of the US Department of Energy developed EnergyPlus (Crawley et al. 2001). The advent of detailed representations of city-scale building stock has allowed the extension single building models to simulate energy demand at district and even city scales (Hong et al. 2016; Olivo et al. 2017; Ahmed et al. 2017). Statistical methods range from linear regression at the simplest levels to machine learning algorithms like support vector machines (Jain et al. 2014) and neural networks (Beccali et al. 2004; Neto and Fiorelli 2008). These methods use historical output (i.e., energy demand or consumption) and input (e.g., outdoor temperature, occupancy rates) variables to train a predictive model. The rise in energy use data due to use of utility smart meters and government reporting requirements has opened the door to predict energy demand at scales from single buildings (Jain et al. 2014; Yan and Liu 2020) to entire cities (Kontokosta and Tull 2017; Chen et al. 2020). An advantage of physics-based models is their reliance on detailed data on building materials, morphology, and technology, which allows study of a wide variety of energy efficiency technologies at the design stage across a variety of use cases and even outdoor climate conditions. Although statistical methods can include these data, they must be selected *a priori* or engineered through feature selection exercises.

A limitation to both of the traditional approaches is their consideration of the building envelope as a standalone entity. In reality, buildings and their surrounding environment are coupled via energy, mass, and momentum exchanges that no only control energy consumption, but often has a significant impact on outdoor climate. AC use is one of the mechanisms leading to the UHI as described above. In order to quantify building-atmosphere dynamics, a method that couples atmospheric and building energy modeling must be used. One way these interactions have been coupled with by embedding building consumption models with numerical weather models. Examples of this approach include the Building Energy Model (Salamanca et al. 2010) and Town Energy Budget (Masson 2000), which parameterize aggregate building energy interactions to a weather model's simulation grid. This approach has been used to simulate energy demand at urban scales in climates as varied as temperate New York City (Ortiz et al. 2018a), arid Phoenix (Salamanca et al. 2013), and tropical San Juan, Puerto Rico (Pokhrel et al. 2018).

Whereas previous work has estimated building energy use at the city scale and its impacts on urban and regional power demand, there has been little research quantifying the burden placed on households by this energy use. In this study we estimate household energy burdens associated with AC operation in cities, using NYC as a case study. We use a numerical weather prediction system coupled to a building energy model to estimate building energy demand at the household scale for an entire city. By employing the coupled weather-building energy model approach, we addresses potentially spatially uneven urban climate change in NYC and its relation to AC energy use, which itself forms a feedback with atmospheric processes due to energy and mass exchanges with buildings. In addition, by modeling the physical interactions between buildings and the atmosphere our study is able to account for synergies between warmer end-of-century summers and urban-scale processes like heat storage and anthropogenic heat generation, which may be missed in statistical-only analyses.

2. Methods

We use a high resolution configuration of the Weather Research and Forecasting model (WRF, Skamarock *et al* 2008) coupled with a modified multi-layer urban canopy and building energy model parameterization to study changes in building cooling demand under climate change conditions. We also characterize indoor heat exposure to highlight potential health risks associated with lack of AC use, as detailed in the following sections. Out modeling approach, with its inputs and outputs are summarize in Fig. 1.

2.1. High resolution urban climate modeling

In order to resolve the fine scale atmospheric processes in NYC, we use WRF to dynamically downscale data from reanalysis for present-day conditions and a GCM for end-of-century climate. The dynamical downscaling technique used here consists of using coarse gridded datasets as initial and boundary conditions to a limited-area numerical weather prediction model that solves the set of equations of atmospheric fluid, mass, and energy in non-hydrostatic form.

Buildings modify the energy and momentum balance at the land surface, with urban morphology and AC use forming feedbacks with the surrounding atmosphere. In order to account for these energy and momentum exchanges between buildings and the atmosphere, simulations use the Building Effect Parameterization (BEP) and Building Energy Model (BEM) physics options in WRF (Martilli et al. 2002; Salamanca et al. 2010). BEP accounts for physical interactions between buildings and the atmosphere such as radiation shadowing and blocking, drag and turbulence effects in the urban canopy, dynamically computing momentum and energy fluxes at all overlapping atmospheric levels. BEM, on the other hand, dynamically computes the building envelope energy balance to estimate energy exchanges between the building and the atmosphere, accounting for conduction through all built surfaces, air mass exchanges, indoor heat generation from humans and equipment, and AC use. The dynamically calculated cooling (or heating) load is used to compute heat fluxes to the atmospheric layers that overlap with embedded BEM parameterization layers at each model time step. For each parameterized building envelope, an energy balance is performed to compute energy fluxes from radiation and advection to and from the urban canopy surfaces (i.e., roof and walls), while the AC subroutine works to remove indoor energy by adding work to the system. As BEP-BEM are a multi-layer urban parameterization, these heat fluxes are computed for as many layers in the atmospheric coordinate system overlap with the building vertical coordinate system. This urbanized version of WRF has been evaluated in cities across a variety of climates like Beijing (Xu et al. 2018), Phoenix (Salamanca et al. 2015), New York (Ortiz et al. 2018b), and the Yangtze River Delta (Liao et al. 2014) to name several examples.

Simulations use three domains (one parent, two nested) with horizontal resolution of 9 km, 3 km, and 1 km (Fig. 2a) and 51 vertical levels, with 15 levels within the lowest 3 km of the atmosphere. The D03 domain resolution of 1 km is set to optimize use of the urban canopy parameters from the NUDAPT1km dataset (Burian and Shepherd 2008) which include spatially explicit sky view factor (SVF), roughness lengths, and frontal area densities at various angles and are in line with similar studies in Chinese cities (Xu et al 2018, Liao et al 2020), the US Southwest (2015), and NYC (Gamarro et al 2020, Ortiz et al 2019, Gutierrez et al 2015).

In order to take advantage of the urban physics parameterizations, additional detailed urban canopy parameters (UCPs) must be used. Here, we derived UCPs from a combination of public NYC tax-lot data, existing gridded datasets, and standards-based look-up tables. Urban land cover and geometry was adapted from the NYC Department of Planning MapPLUTO dataset (New York City Department of City Planning 2020), which provides heights and footprint areas of buildings at the tax-lot scale (Fig. 2b-c). The tax-lot data was aggregated to the D03 domain's 1 km grid, with mean values of building height, surface-to-plant are ratio, and building area fraction. Urban land use was aggregated into three categories: low density residential, high density residential, and commercial/industrial based on the land use field in

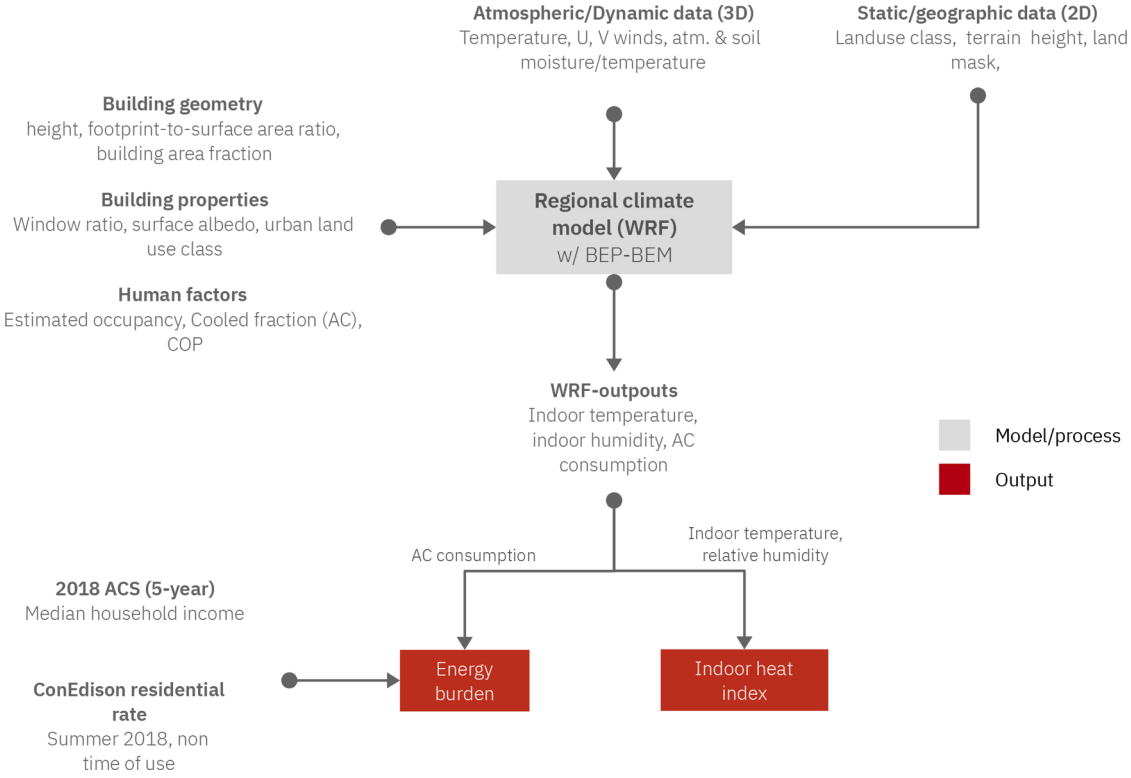

Fig. 1. Experimental workflow detailing key inputs and outputs used to produce energy burden and indoor heat index.

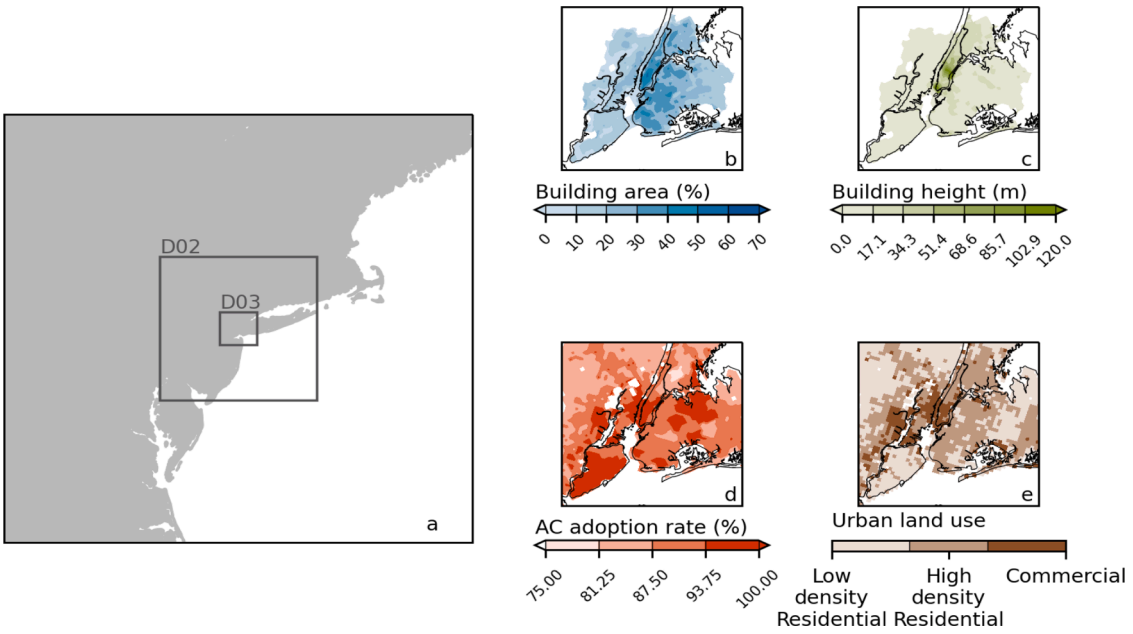

Fig. 2. (a) WRF parent domain (map extent, 9 km resolution) configuration with nested domains D02 (3 km resolution) and D03 (1 km resolution). Urban parameters added to simulations include (b) grid building area fraction, (c) grid average building height, (d) grid AC adoption rate, and (e) urban land use classes.

MapPLUTO (Fig. 2e), following the encoding detailed in Gonzalez et al (2017). Urban land use aggregation used the most common land use found in each 1 km grid cell.

Panel Fig. 2d shows the spatial distribution of the fraction of homes with AC units from Ito et al (2018), used in analysis of vulnerability to indoor extreme heat and AC energy cost burdens, detailed in in section 2.. Other parameters like roughness lengths were extracted from the default NUDAPT 1 km database for NYC (Burian and Shepherd 2008). In addition, building AC use has been updated in BEM to partition heat fluxes into both latent and sensible components by including evaporative cooling processes (Gutiérrez et al. 2015a). This approach accounts for evaporative cooling used in modern AC systems and applied to the entire domain. BEP was also modified to include a variable drag coefficient as a function of building area fraction based on a set of fluid dynamics experiments (Santiago et al. 2008; Gutiérrez et al. 2015b).

Other parameters directly used by BEM (Table 1) follow previous work (Gutiérrez et al. 2015a; Ortiz et al. 2018a), which modify the urban parameter lookup table with values better aligned with recommendations by the American Society of Heating, Refrigerating and Air-Conditioning Engineers (ASHRAE). The use of constant lookup table values are a simplifying assumption that building parameters are relatively uniform across urban landuse classes. These constant parameters ignore some of the variations in building construction and AC technologies (e.g., COP differences between window and central AC) across the city and present an opportunity to further refine future simulations.

Table 1
Urban canopy and building energy parameters from the WRF lookup table.

Urban Parameter	Value
Temperature set point (°C)	22.22
Humidity set point (kg_{vapor}/kg_{air})	0.01
Coefficient of performance	2.8
Window area fraction	0.33
Roof albedo	0.2
Roof emissivity	0.9
Peak equipment load (W/m^2)	16.0/20.0/26.0
Peak occupancy ($person/m^2$)	0.025/0.025/0.050 (Low density res./High density res./ Commercial)

These parameters include broad descriptions of building surface properties like roof emissivity and window area coverage, as well as characterizations of the building envelope. The latter include peak occupancy and electronic equipment loads, as well as the AC coefficient of performance, which is defined as the the ratio of the heat removed from the building to the atmosphere (i.e., from the hot reservoir to the cold reservoir) to the amount of work required to remove it. Other parameters include AC configurations for temperature and humidity which are often configurable by end users of building engineering staff on a day to day basis but remain static in the simulations performed here.

Other physics options were selected following previous work over the NYC region and are detailed in Table 2 (Ortiz et al. 2019). Simulations were carried out at a high performance computing facility, with each model run using 128 processors and using approximately 7 days of compute time. The high performance computing system uses Intel Sandy Bridge architecture processors, organized in 16-core nodes.

Table 2
Model physics parameterizations used in WRF simulations.

Model Physics	Parameterization
Land surface model	NOAH LSM (Tewari et al. 2004)
Cumulus	Kain-Fritsch (Kain 2004), off in D03
Microphysics	Thompson (Thompson et al. 2008)
Urban canopy	Building Effect Parameterization (BEP) (Martilli et al. 2002) Building Energy Model (BEM) (Salamanca et al. 2010) AC Evaporative Cooling Parameterization (Gutiérrez et al. 2015a) Variable Urban Drag Coefficient (Gutiérrez et al. 2015b)
Shortwave radiation	RRTMG (Iacono et al. 2008)
Longwave radiation	RRTM (Mlawer et al. 1997)
Planetary boundary layer	Mellor-Yamada-Janjic (Janjić 1994)

2.2. Simulation design

To study the impacts of warming climate conditions on demand-side AC costs, we use a typical, relatively recent summer, referred to here as PRESENT, then find its future analog based the distribution of daily minimum, mean, and maximum temperatures. To select a typical summer, we used historical daily maximum temperature records from the Central Park weather station between the years 2089-2019 and calculated the yearly minimum, mean, and maximum daily peak temperatures. Summer 2018 exhibited the closest to typical (i.e., 50th percentile) values of these metrics of any of the previous 10 years (Table 3).

The analog is found by use of the Central Park weather station. Then, we find the yearly minimum, mean, and maximum of daily maximum temperature, as well as its percentile rank in the 30-year period ending in 2018. For the future analog, we find the same yearly statistics in global model data for the 2070-2099 period, then find the year that lies closest to the percentile rank of summer 2018. The closest year is found by finding the year with the minimum Euclidean distance to the chosen recent summer, as follows:

$$FUTURE = MIN\left(\sqrt{\left(T_{min,2070-99} - T_{min,i}\right)^2 + \left(T_{mean,2070-99} - T_{mean,i}\right)^2 + \left(T_{max,2070-99} - T_{max,i}\right)^2}\right)$$

Here, $T_{min,2070\text{-}2099}$, $T_{mean,2070\text{-}2099}$, $T_{max,2070\text{-}2099}$ represent the yearly daily maximum temperature minima, mean, and maxima, respectively, while the subscript i denotes a particular year. The year with the closest matching temperatures was 2097, referred to from here onward as the FUTURE period, as shown in Table 3. PRESENT simulations use the North American Regional Reanalysis (NARR, Mesinger *et al* 2006) as initial and boundary conditions, while FUTURE simulations use a bias corrected Community Climate System Model version 4 (CCSM4) business as usual RCP 8.5 as initial and boundary conditions (Monaghan et al. 2014). NARR is a high resolution reanalysis product covering the North America and the Caribbean with a 32 km grid resolution and 29 vertical levels. CCSM4 is a general circulation model that couples an atmospheric, ocean, and ice sub-models to project future climate scenarios. The particular CCSM4 simulations used here are part of the fifth Coupled Model Inter-comparison Project (CMIP5) and use 26 vertical levels at 1° x 1° horizontal resolution. Both of these these initial and boundary conditions provide a coarse information on the region's winds, sea surface temperatures, and atmospheric and soil temperature and moisture content. As a result, our simulations account for changes in climatic conditions as a result of the global climate signal for all variables as modeled by the CCSM4 output. Table 4 summarizes the geospatial data inputs used as parameters as well as initial and boundary conditions used in all simulations. In order to model indoor heat exposure, a second set of PRESENT and FUTURE simulations were performed with 0% AC adoption. For these simulations, all AC-related heat fluxes are set to 0, while still allowing for the computation of other heat fluxes to and from buildings related through indoor generation, radiative transfer and advection.

Table 3
Minimum, mean, and maximum of daily maximum temperatures of Summer 2018, and their percentile rank between 1989-2018 based on the Central Park weather station. FUTURE summer 2097 is selected from CESM1 data between 2070-2099 at the same percentile ranks.

	PRESENT	Percentile	FUTURE
$Tmax_{min}$	21.2°C	73rd	27.1°C
$Tmax_{mean}$	28.6°C	53rd	35.2°C
$Tmax_{max}$	34.6°C	43rd	42.5°C

Table 4
WRF simulation model inputs and urban canopy parameter source data.

	Present	Future
Initial and boundary conditions	North American Regional Reanalysis (32 km resolution)	CCSM4 (1° resolution)
Urban Canopy Parameters (geometric)	MapPLUTO (tax-lot resolution)	
Urban Canopy Parameters (non-geometric)	NUDAPT1km (1 km resolution)	

A third simulation, set in the PRESENT time period, uses the data from Ito et al (2018) as a measure of current AC adoption in NYC, shown in Fig. 2d. AC adoption rates are included in the model by modifying the indoor energy balance in each urban-category grid cell by the fraction of homes with AC in BEM based on work exploring environmental and infrastructure impacts of AC adoption in NYC (Gamarro et al. 2020):

$$H^p_{out} = H_{out} * \alpha$$

$$E^p_{out} = H_{out} * \alpha$$

$$E_c = \frac{1}{COP}\left(H^p_{out} + E^p_{out}\right)$$

Here, H_{out} and E_{out} represent the building sensible and latent heat fluxes, E_c is the cooling electric demand, α is the AC fraction, and superscript p denotes variables that account for fractional AC use. One limitation of this approach is the use of the same cooled fraction for all urban land uses, including commercial. However, due to the 1 km resolution of the model configuration combined with the city's household income spatial distribution, majority commercial land use grids coincide with the highest AC adoption rates at nearly 100%, which may be in line with commercial cooling practices. Results from this simulation are used to evaluate model performance against weather station data.

2.3. Energy burden and heat exposure indicators

To estimate energy burden, we use the AC demand output from BEM in our WRF simulations, census block group income data, and pay scales from the local utility, Consolidated Edison. AC demand is dynamically calculated in BEM and used by the model to estimate anthropogenic heat fluxes. We estimate the energy burden associated with AC use as:

$$Burden_{energy} = \frac{Cost_{AC,household}}{Income_{household}}$$

where $Cost_{AC,household}$ is the electricity cost related to cooling 100 m^2 per grid point and $Income_{household}$ is the median income of a household derived from the American Community Survey (ACS) 2017 5-year estimate. We obtained the energy cost by multiplying hourly AC demand from BEM and Consolidated Edison schedule 2 rates with no time-of-day pricing. The summer (i.e., schedule 2) rate for the 2018 May-September period was 0.2493 US $ / kWh, which includes charges for generation, transmission, and local taxes, The energy consumption was obtained on a per-grid cell basis from BEM, which computes cooling loads in units of W/m^2. We scaled the load to a 100 m^2 dwelling in order to provide burden values for a typical home size. Since ACS data is released at the

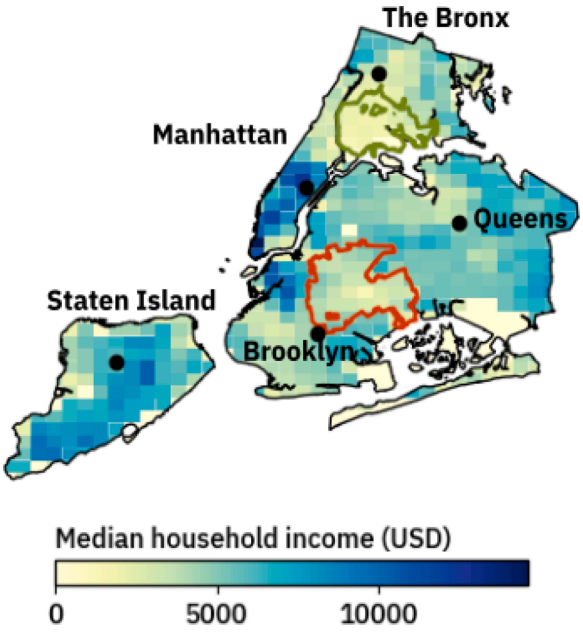

Fig. 3. 5-year median household income estimate from the 2017 ACS, interpolated to WRF simulation grid. Green boundary represents the South Bronx region, while the orange boundary encloses East and Central Brooklyn. Black circles show locations of NYS Mesonet stations used in model evaluation.

irregular census block group scale, it is interpolated to the regular 1 km resolution grid used in WRF simulations (Fig. 3).

Table 6

This study estimates potential exposure to hazardous heat conditions using the indoor heat index. This potential exposure is calculated using a WRF simulation in which AC is turned off to explore the geospatial distribution of heat exposure when no cooling is available. The heat index (Steadman 1979) is a measure of "felt" or "apparent" temperature as experienced by humans that combines temperature and relative humidity. Originally developed as a table relating wet and dry bulb temperatures to heat index, it has since been adopted by the U.S. National Weather Service (NWS), usually using relative humidity and air temperature. Here, heat index is estimated via the method used by the NWS based on the regression from Rothfuz (1990). The regression equation takes the following form

$$HI = C_1 + C_2T + C_3RH + C_4T*RH + C_5T^2 + C_6RH^2 + C_7RH*T^2 + C_8T*RH^2 + C_9T^2*RH^2$$

where C_i are the regression coefficients:

$$C_1 = -42.379$$
$$C_2 = 2.04901523$$
$$C_3 = 10.14333127$$
$$C_4 = -.22475541$$
$$C_5 = -6.83783x10^{-3}$$
$$C_6 = -5.481717x10^{-2}$$
$$C_7 = 1.22873x10^{-3}$$
$$C_8 = 8.5282x10^{-4}$$
$$C_9 = -1.99x10^{-6}$$

and the variables T and RH are indoor temperature in degrees Fahrenheit and relative humidity in percentage units from the BEM parameterization, respectively. Indoor temperature and relative humidity were averaged for all urban vertical levels, and the estimated heat index was assigned as a bulk per-grid point value. In addition, if RH is less than 13% and T lies between 80-112°F (26.67-44.44°C), an adjustment is subtracted from HI as follows:

$$ADJ = (13 - RH)\Big/4\sqrt{17 - |T - 95|/17}$$

If, however, RH is greater than 85ˆ and T lies between 80-87°F (26.67-30°C), the adjustment term below is added to HI:

$$ADJ = (RH - 85)/10 * (87 - T)/5$$

Finally, if the above process yields a HI value below 80°F (26.67°C), the following equation is used instead, without additional adjustments:

$$HI = 0.5[T + 61 + (T - 68)*1.2 + RH*0.094]$$

Although the original formulation of the heat index was parameterized to include the impacts of clothing layers and skin heat transfer processes (e.g., convection, evaporation, and radiation), NWS adoption uses a series of assumptions such as light breeze (5 knots, or ~x223C 2.5 m/s), light clothing (short-sleeved shirt) and shaded conditions to facilitate development of warning systems, which are somewhat similar to indoor environments. The wind speed assumption used here is consistent with wind speeds commonly associated with ceiling fans in residences (Schmidt and Patterson 2001; Aynsley 2006). This formulation of the heat index computed with indoor values has been linked to higher incidence of cardiovascular and respiratory illness (Uejio et al. 2016), particularly among vulnerable populations in NYC (e.g., the elderly), and has been used to study indoor heat exposure during extreme heat events (Quinn et al. 2014). Although work by van Loenhout et al. (2016) found that heat index provided no additional predictive value when assessing heat-related impacts in elderly populations, they pose that this may be due to the relatively temperate conditions in their study and be of more use in warmer, more humid climates.

To estimate exposure of populations to hazardous heat conditions, we partition heat index values using the classification bands used by the NWS, then compute the number of hours when the heat index is in the *Very Hot* or higher (heat index > 40.6°C). These categories are of particular significance, as they are used by NWS and the NYC Department of Health to issue public warnings. Although authorities issue these warnings based on outdoor measurements, studies have shown that in the absence of air conditioning, temperatures decrease at a slower pace indoors compared to outdoors due to heat storage in building materials and lack of ventilation (Vant-Hull et al. 2018), increasing heat exposure relative to the outdoors.

Table 5
Albedo and target temperature values used in adpatation strategy sensitivity simulations. Items in bold font mark the high end adaptation used in the full summer simulations.

	Roof albedo	Target temperature / spec. humidity
Baseline	0.2	22.2°C (0.001 kg_{vapor} /kg_{ai})
Albedo sensitivity	0.4	22.2°C (0.001 kg_{vapor} /kg_{ai})
	0.6	22.2°C (0.001 kg_{vapor} /kg_{ai})
	0.89	22.2°C (0.001 kg_{vapor} /kg_{ai})
Target temperature sensitivity	0.2	23.3°C (0.001 kg_{vapor} /kg_{ai})
	0.2	24.4°C (0.001 kg_{vapor} /kg_{ai})
	0.2	25.0°C (0.002 kg_{vapor} /kg_{ai})

Table 6
Location and error statistics for WRF simulations using Partial and full AC adoption.

Name	Latitude (°)	Longitude (°)	Partial AC RMSE (°C)	Full AC RMSE (°C)
Brooklyn	40.631762	-73.953678	3.10	3.18
Bronx	40.872481	-73.893522	2.83	2.90
Manhattan	40.767544	-73.964482	2.88	2.91
Queens	40.734335	-73.815856	3.09	3.20
Staten Island	40.604014	-74.148499	2.98	2.96

2.4. Adaptation strategies

One way to offset energy usage increase from full AC adoption is widespread implementation of technologies like reflective roofs or higher AC set point values. The former can reduce energy demand by reducing radiative energy fluxes into the building envelope through the roof, while the latter reduces the cooling load by narrowing the indoor-outdoor temperature difference. We estimate potential reductions to energy burden via a second set of simulations implementing these two approaches.

We also use a set of 1 month simulations to study the sensitivity of the energy burden indicator to increases in roof albedo and target temperature and humidity. The simulations use the same input data and physics parameterizations as the base simulations, but run for only for July rather of the full summer to accommodate a larger. Table 5 details the roof albedo and AC target temperature combinations used in the sensitivity simulations. Finally, a second set of adaptation simulations using properties from high end reflective roof coatings and warmer indoor conditions are run for the entire 2018 summer perior. These two simulations use a building roof albedo (i.e., reflectivity) to 0.89 represent the high end of commercially available technology (as per a review of commercial reflective roof coatings). In the second set of simulations, we change the temperature and humidity set points of the model AC to the upper of ASHRAR standards (ASHRAE 2017) for thermal comfort (25°C and 0.2 kg_{vapor} / kg_{air}).

3. Results

3.1. Model evaluation

To evaluate model performance, we compare simulation results with temperature observations from the New York State Mesonet network, and estimated AC peak load demand from the New York Independent System Operator (NYISO). NYISO is a nonprofit, quasi-governmental entity tasked with managing the state of New York's electric supply market. As part of the services it provides, it reports electric loads for each of the New York State load zones, of which NYC is one. To evaluate model performance in reproducing temperatures, a weather station was selected from each of the city's five boroughs (Brooklyn, The Bronx, Manhattan, Queens, and Staten Island), collecting data at 2 m height above ground. Then, the closest model grid point is selected and compared against each stations' recorded hourly temperatures.

Comparisons against the weather stations reveal that root mean square errors (RMSE) in simulations with present-day AC adoption rates ranging from 2.83-3.10°C. Errors are largest during nighttime, particularly when temperatures remained warm overnight (above 22°C), and simulated temperatures dropped to below 17°C. When considering full AC adoption, which in some neighborhoods represent an increase of around 25% AC adoption, RMSE is slightly higher in all boroughs except Staten Island. Although model improvement is modest when considering partial AC fractions, results are consistent with previous work by Xu et al (2018), which adopted a per urban class fractional cooled fraction for the city of Beijing.

NYISO records total electric load for NYC at 5 minute intervals, which we resample to hourly mean values. Since NYISO reports supply-side electric loads, its values include signals related to transmission and distribution losses, lighting, transportation, and other non-AC energy use. We refer here to the loads not related to transmission losses as the base load. To disaggregate the total load for a closer comparison to the simulated AC electric load, we first account for transmission and distribution losses as well as the baseline (i.e., non cooling) loads.

We account for transmission and distribution losses by dividing hourly values by a loss factor of 6.67%. This load factor was obtained from the report on grid losses by the New York State Energy Research and Development Authority, using the state average as an approximation (Short and Swayne 2012). Then, we follow the methods detailed by Salamanca et al (2013) to separate electric loads into two components: one driven by meteorology (i.e., AC loads) and the other by human

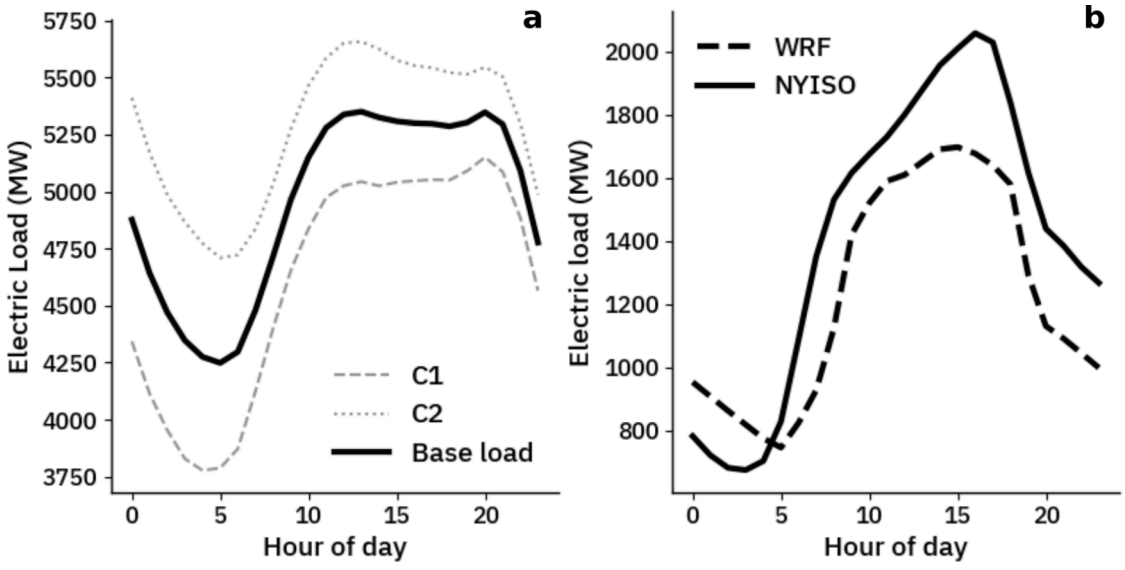

Fig. 4. (a) Hourly daily base load for and its two components and (b) Hourly daily AC electric loads for summer 2018 estimated from WRF simulations and NYISO supply-side load.

behavior (i.e., base loads). To estimate this human behavior component of the electric load, we extract the data from the day with the lowest load (C1) and the day with the lowest diurnal range (C2), defined as the difference between the daily maximum and minimum load in a given day. The base load is then computed from the average between these (Fig. 4a):

$$Baseload = \frac{C1 + C2}{2}$$

Simulated AC demand from the Partial AC adoption simulation is clipped to the NYC boundary, then all grids are added to obtain hourly AC load. Comparing the disaggregated NYISO AC electric load with WRF simulated loads (Fig. 4b) for average per-hour values, we find generally good agreement, with a root mean squared error of 209 MW, or about 15.8% of the mean daily load. Differences between WRF and NYISO are largest in the afternoon peak and lowest in the early morning. This lower sensitivity of the WRF AC load to outdoor conditions might be due energy fluxes into buildings being too low as a result of some of the lack of detail in some of the lookup table parameters (e.g., roof and wall conductivity, emissivity) or underestimating temperature set points (e..g, commercial and office spaces might be overly cooled). The daily cycle also follows a similar hourly progression, albeit with a 1-2 hour lag at the beginning of the work day, with a small peak in the morning (10AM) and a larger peak in the late afternoon (3-4PM).

We note that the use of a bulk supply-side dataset to evaluate NYC-wide cooling loads presents challenges. We have mitigated this issue with two considerations here. As simulations only run for the NYC summer season (June-July-August) they are unlikely to encounter days where heating is active (indeed, mandatory heating season in NYC ends in May). Second, the method used to compute the baseline load uses the average of the days with smallest load, which arguably should have the least cooling or heating as well as the day with the smallest daily diurnal range to approximate its non-weather dependent. These two days were May 14, 2018 and June 10, 2018 which had peak temperatures of 21°C and 22°C, which are very close to standard temperature set points, and when we can assume cooling and heating loads to be negligible. In addition, there were no massive disruptions in public transportation or power outages during these days, ruling out extreme or anomalous baseline loads. In addition, differences in infrastructure use and actual AC usage may add uncertainty. Another point of uncertainty in simulated AC is that all urban grid cells are cooled unless the AC fraction parameter is zero. Additional data on building materials and AC performance may make these results more in line with observations and sensitive to the day to day weather variation.

3.2. Indoor heat exposure

Fig. 5 shows indoor heat exposure, presented as the percent of summer (June-July-August) hours that reach or exceed 40.6°C. In the PRESENT simulation (Fig. 5a), heat index meets or exceeds the *Very Hot* treshold between 10 and 70 percent of days. Locations near midtown and downtown Manhattan, where commercial landuse uses half as much occupancy than in residential areas (Fig. 2b-c), experiences the fewest hours of exposure. Locations with highest hours of exposure are characterized by residential units where occupancy is double that of commercial land use, as shown in Fig. 2e and Table 1. As occupancy acts as a source of sensible and latent heat in BEM, this leads to significant differences in the indoor moist air enthalpy across the city (SI Fig. 4). A less intense spatial gradient of hot temperatures is also consistent with previous characterizations of the NYC UHI, with an afternoon breeze cooling southern areas of NYC and moving the core of the UHI to the northwest Bronx and upper Manhattan (Gedzelman et al. 2003). These results, however, only capture days between June 1 – August 31, which caps the number of hours to 2208 (92 days, 24 hours each).

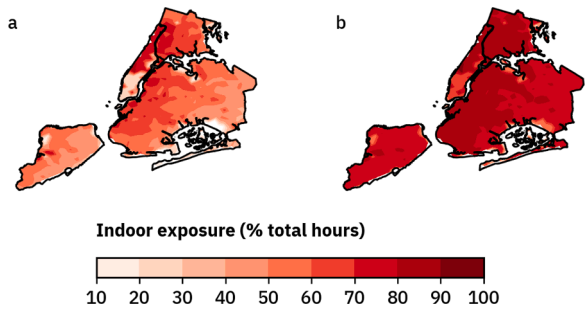

Fig. 5. Percent of summer (JJA) hours when indoor heat index reaches or exceeds Very Hot threshold in the (a) PRESENT and (b) FUTURE simulations.

3.3. Energy Burden

Results show that AC Burden varies across NYC, with values in the PRESENT simulation ranging from near zero to over 2% of total income per 100 m^2, with 99th percentile value of 2.4% per 100 m^2. In the PRESENT simulation (Fig. 6a), highest burden areas are located in the South Bronx and Easter/Central Brooklyn (boundaries shown in Fig. 3). Relatively low incomes drive these high burden areas, with the lowest income households earning under 2500 USD per month, which is lower than the NYC published poverty threshold of 32402 USD annual income (New York City Office of the Mayor 2017). Grids within the south Bronx are particularly notable, as they both experience the highest share of summer hours above 40.6°C, and the center of afternoon outdoor UHI as shown by Gedzelman et al (2003). Meanwhile, high incomes in most of Manhattan (> 10000 USD per month) lead to relatively low energy burden of less than 0.1% income per 100 m^2. These burdens could be, however, significantly lower for high income households, as ACS income brackets stop at 250000 USD annual income, skewing collected survey data.

In the FUTURE simulation (Fig. 6b), AC burden increases in all grids as a function of warming summer temperatures. Although mean energy burden for the entire city is 0.9% income per 100 m^2, the lowest income neighborhoods experience up to 8% income per 100 m^2. Meanwhile, the top 1% of grids have a burden of 3.2% income per 100 m^2. Since energy burden calculations do not consider income changes, grids with highest burden values remain in the present-day low income neighborhoods. Changes between FUTURE and PRESENT (Fig. 6c) show that AC burden increases are larger in already vulnerable areas. These areas also coincide with the neighborhoods with lowest AC adoption rates (Fig. 2d) and household income (Fig. 3). There is an inverse relationship between the change in AC burden and monthly income, with higher income areas experiencing less than 4 times the increase in burden (Fig. 9). Although relative costs of AC increase at higher rates in these regions, they also experience the longest projected hours exposed to *Very Hot* conditions when no AC is used. AC burden change varies with building characteristics.

Urban form and building properties also have an impact on thermal loading and outdoor conditions, as has been which in turn may impact indoor climates. In general, more densely built areas (Fig. 7a) with less less tall (Fig. 7b) buildings experience the largest increases in AC burden. The tallest, most slender buildings (i.e., with high ratio of total surface area to footprint area, Fig. 7c), like those found in the large commercial districts in the city experience almost no increases in AC burden over time. However, without accounting for those buildings, AC burden increases with increasing surface to plan area ratios. A similar pattern is observed built area fraction, where the very highest burdens lie in regions with relatively low built-up area. These patterns may be due to differences in neighborhoods populated with large single-family homes versus other areas with densely packed multi-family housing that is common in less lower income areas like the south Bronx and upper Manhattan.

We also quantify changes in indoor thermal heat using moist

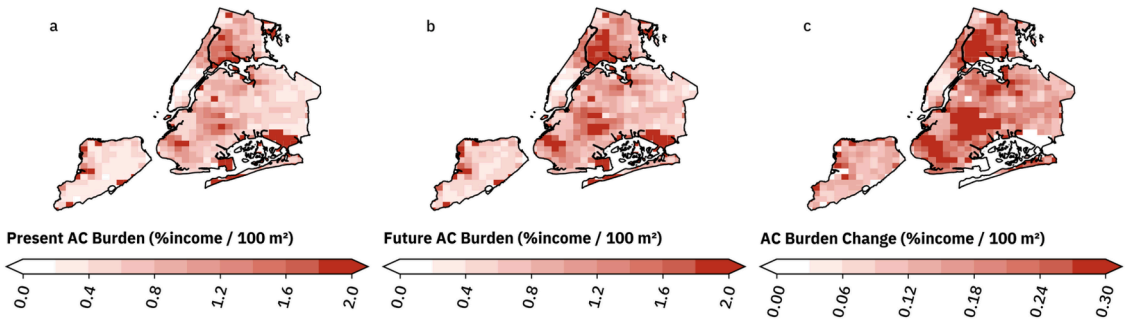

Fig. 6. AC utility cost burden for the (a) PRESENT and (b) FUTURE simulations, as well as (c) the difference between the two.

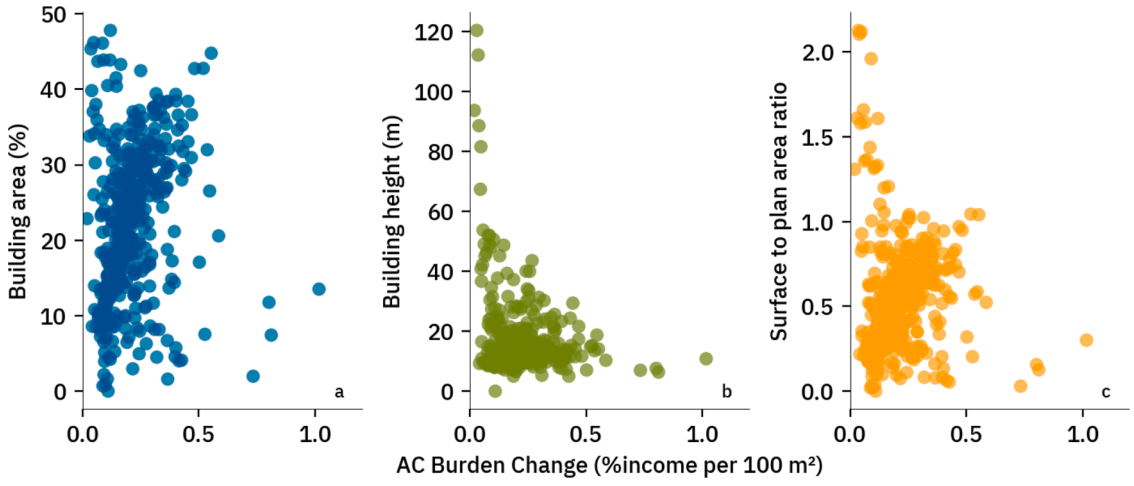

Fig. 7. Scatter plots of AC burden change against grid (a) building area fraction, (b) building height, and (c) building surface to plan area.

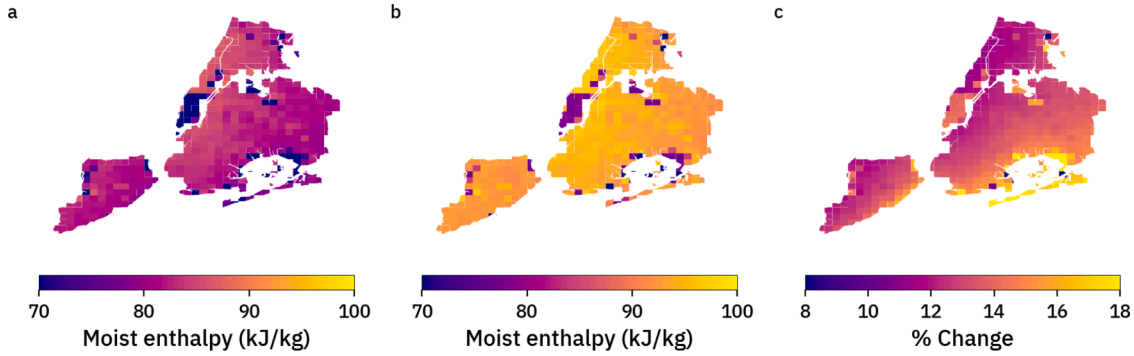

Fig. 8. Mean indoor moist enthalpy for (a) PRESENT, (b) FUTURE, and (%) the percent change between them.

enthalpy. We estimate moist enthalpy using the ASHRAE approximation (American Society of Heating 2017):

$$h = 1.006T + q(2501 + 1.805 * T)$$

Here, h is the indoor moist enthalpy, T is the indoor temperature, and q is the indoor specific humidity. Simulation results (Fig. 8a-b) show that the geospatial pattern is mostly influenced by the urban land class (Fig. 2e), with distance to the coast playing a smaller role. Although buildings in commercial landuse have lower moist enthalpy than those of the two residential urban land classes, they experience a slightly higher percent change between PRESENT and FUTURE simulation, close to 2% higher (Fig. 8c). Areas with low relative change coincide with low income neighborhoods where the energy burden and its projected increase is also highest, so we conclude that household income is the main driver of the energy burden in NYC.

These results highlight some of the impacts important to discussions of heat adaptation measures. Although low income neighborhoods experience the longest exposure time to indoor extreme heat, they also see the highest relative costs of AC operation. Warmer end of century summers exacerbate the differences between high and low income groups both in terms of indoor heat exposure and utility costs. Previous work has shown that periods of increased spending on heating during cold weather negatively impacts spending on food in low income families (Bhattacharya et al. 2003). Barring any economic assistance to offset increasing cooling costs, increasingly hot summers may have a similar impact on household budgets, lowering health outcomes either by reduced food or reduced cooling spending.

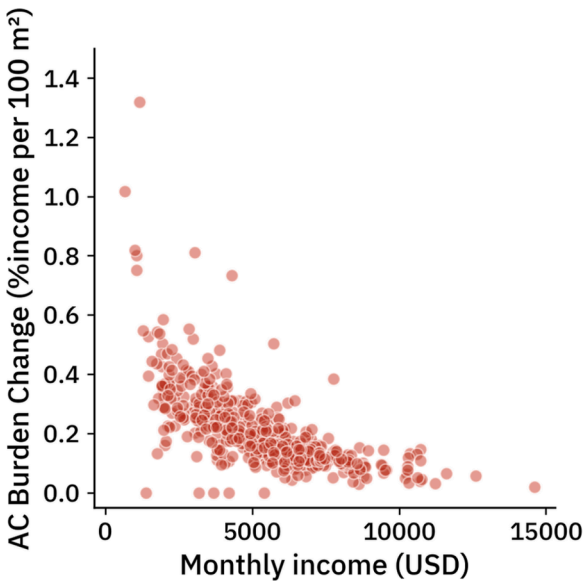

Fig. 9. Grid-point change in AC burden between the PRESENT and FUTURE simulations as a function of 2017 ACS income.

3.4. Energy burden reduction strategies

Results from the sensitivity analysis is summarized in Fig. 10. Overall, results show decreasing burden as adaptation magnitude increases, with increases in set point resulting in the largest decreases in burden. Median energy burden for the albedo simulations (Fig. 10a) range from 0.80 %income/100 m^2 in the baseline simulation to 0.62 % income/100 m^2 in the maximum adaptation scenario. However, impacts are significantly larger in high burden locations, with burdens going from 8.7%income/100 m^2 in the baseline simulation to 6.7 %income/100 m^2 in the maximum albedo simulation. Energy burden is more sensitive to changes in set point (Fig. 10b), with median values going from 0.80 %income/100 m^2 in the baseline case to 0.53 %income/100 m^2 in the maximum. In the highest burden locations, the energy burden range from 8.7 %income/100 m^2 to under 5.5 %income/100 m^2. Running a linear regression with the results of the sensitivity study, we find that on average energy burden decreases by 0.002 %income/100 m^2 per unit increase in albedo, and 0.06 per unit increase in set point, with both trends being statistically significant ($p < 0.001$).

Results from our two adaptation strategy simulations show that adaptation strategies can have significant impacts on the cooling energy burden at the household level (Fig. 11). Increasing the AC temperature and humidity set points have the largest impacts throughout the domain, with the burden in the South Bronx region decreasing by 0.33 % income per 100 m^2 on average, a reduction of nearly 21%. We find the burden in East Brooklyn area decreased, on average, by 0.24 % income per 100 m^2, or 20% of their future burden. In some grid cells, percent reduction in burden reaches close to 0.50 % income per 100 m^2 or up to 22% of the total future burden within both boundaries.

Results from the reflective roof simulations show relatively modest reductions in energy burden compared to raising AC set points. For instance, reductions in cooling energy burden averaged in the South Bronx 0.13 and reaches up to 0.21 % income per 100 $m^{2,}$ representing decreases of 8% and 10%, respectively. Meanwhile in the East Brooklyn area, reductions averaged 0.8 % income per 100 m^2 and up to 0.15 % income per 100 m^2, representing decreases of 6% to 13% of their total.

These results are consistent with recent work in by Mughal et al (2020), which found larger reductions in cooling energy demand from increasing set points from 21°C to 25°C than from reflective roof coatings. They found, however, that cool roof coatings decrease outdoor temperatures in low-rise areas more than set-point increases do, which might provide benefits beyond the building envelope.

4. Conclusion

Through a series of coupled building energy-weather simulations combined with census and utility data, we present an estimation of the burden of indoor cooling relative to household incomes in NYC. To the authors' knowledge, this is one of the first studies that contextualizes dynamically modeled energy use with spatially explicit household income data at the city scale. By modeling the physical processes between buildings and the atmosphere, our work accounts for the feedbacks inherent to the urban climate system that impact the thermal loading of buildings, which in turn has an important role in cooling costs.

We compare these costs by using hours exposed to hazardous heat as an indicator of heat-related health risks. In addition, we present potential climate-driven impacts of warming summers to this cost. Our results show that locations with lower income households have the highest estimated energy burden from AC use. In locations with the highest burden, under present climate conditions, a 100 m^2 household would spend 6.1% of their total income on cooling during a fairly typical

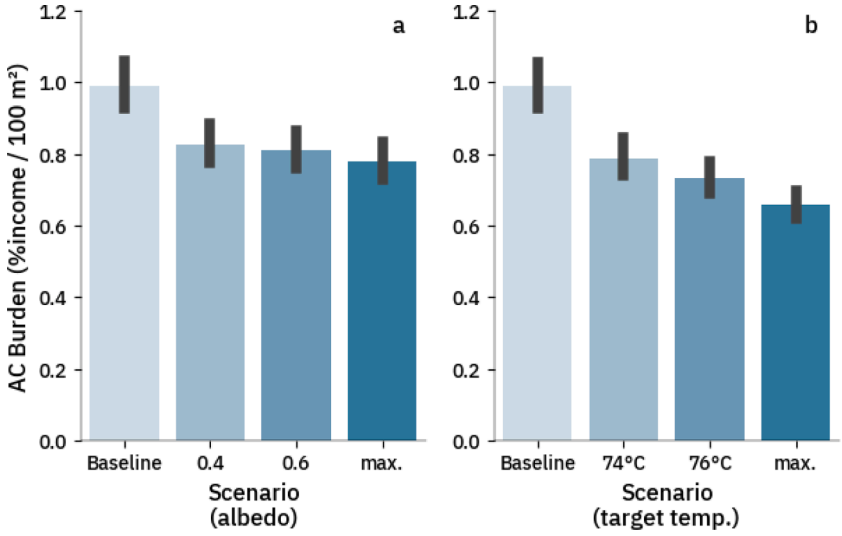

Fig. 10. Sensitivity of AC energy burden for (a) increases in rooftop albedo and (b) increases in AC set point temperature. Black bars represent a bootstrapped 95% confidence interval using 1000 bootstrap iterations.

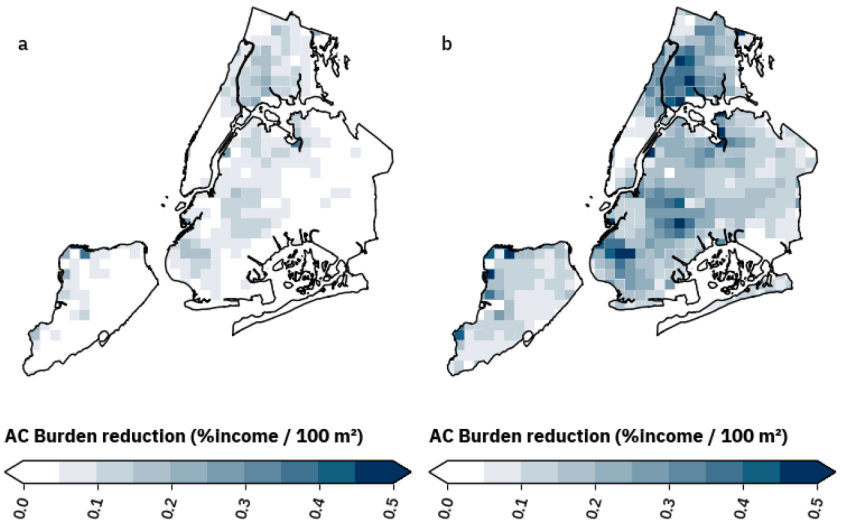

Fig. 11. AC Burden reduction resulting from (a) full adoption of reflective roof coatings, and (b) higher set points.

summer. Meanwhile, during an equivalent end of century summer in a high emissions scenario, this cost could increase to 8% of total income. These locations coincide with neighborhoods recorded to currently have the lowest AC adoption rates and highest heat mortality rates (Ito et al. 2018). Work by Madrigano et al (2015a) also found that these neighborhoods have high rates of vulnerable populations (elderly, low income) (Madrigano et al. 2015a). Their work found that mortality rates increases during a heat wave were higher for low income, non-white, and elderly populations in NYC compared to other groups. This uneven exposure across vulnerable populations was compounded by less accessible green space and higher neighborhood surface temperatures, a trend that has recently been found across many US cities as recently found by Hsu et al. (2021).

Meanwhile, energy burden in higher income neighborhoods range from nearly negligible ($<$ 0.01% of total income per 100 m^2) to 0.5% of total income 100 m^2, with current AC adoption rates close to 100%. We also show that changes in the energy burden are higher in low-income areas in spite of lower relative increase of internal heat load compared to higher income neighborhoods.

Simulated exposure to indoor heat and AC energy burdens are driven by indoor parameters like occupancy, building infrastructure and meteorological processes. NYC summer temperatures are often characterized by an afternoon sea breeze from the south east which significantly cools areas in proximity to the coastline while essentially moving the core of the daytime UHI northwest and into parts of New Jersey, which contributes to the indoor temperature gradient reproduced by our simulations. Previous studies also show vertical variation in indoor temperatures, with top floors, even in tall buildings, can have significantly higher temperatures than ground floor dwellings, which is not considered in our analysis (Quinn et al. 2017).

High costs of air conditioning operation may also serve as a driver of passive, less energy intensive forms of building envelope cooling. Studies have shown that cool roofs (e.g., white roofs and green roofs) and even photovoltaic panels can decrease cooling loads significantly (Jaffal et al. 2012; Skelhorn et al. 2016; Salamanca et al. 2016) during the warm season. Rooftop technologies might be particularly useful in the high-burden neighborhoods with the largest indoor heat exposure as their shorter, less slender can deflect a more significant portion of incoming solar radiation via roofs (Ortiz et al. 2016), with estimated reductions of 10-16%. Our work presented here, however, highlights how these technologies may benefit low-income communities, with potential reductions of up to 20% in an idealized adoption scenario. In addition, urban planning and use of urban gardens and other vegetation have been shown to reduce not only outdoor temperatures (Dimoudi et al. 2014; Farhadi et al. 2019) but also reduce energy poverty (Tsilini et al. 2015).

4.1. *Limitations and uncertainty*

One of the largest sources of uncertainty in our work is the consideration of static social indicators (e.g., population, median income). Although results show increase in indoor heat exposure hours under no AC use, we do not account for changes in populations, income, or building infrastructure throughout the 21st century. Therefore, results should be interpreted as potential impacts on current NYC conditions. These uncertainties are partly constrained by the recently reported slowdown of population increase in NYC (U. S. Census Bureau 2019). In addition, as income and population data from the American Community Survey 5-year estimate are derived from somewhat limited samples, as opposed to the comprehensive decennial census, they carry margins of error. In our analysis, each grid point is assigned the median value to estimate economic burden, whereas income might vary drastically between households within a single neighborhood or even city block. Occupant behavior, which is not accounted for in this study, can also significantly impact both energy use and hazardous heat exposure, as people may move to outdoor activities as a function of outdoor weather conditions or typical day-to-day activity. In addition, model evaluation as performed here is limited by a lack of spatially explicit building electric load data and the method used to compute the non-weather sensitive of NYISO bulk supply-side data.

Another limitation of the study relates to the use of electric rates from a single summer. Utility rates vary year-to-year due for various reasons, including taxes on generation and transmission, repair and maintenance of infrastructure, and projected electric demand. Based on Consolidated Edison approved rate increases, NYC residents will be seeing cost per kWh to grow by nearly 4% per year until 2022 (Consolidated Edison 2021a). Nevertheless, rate hikes may change at different dates due to changes in energy supply and new investments in energy infrastructure. Further, there has been increased focus from utilities to offer “Time of use” (TOU) pricing, where energy use is more expensive during peak demand times. These TOU pricing schemes usually charge less than current averages during off-peak hours, but may charge significantly more during peak or so called “super-peak” hours (Consolidated Edison 2021b). These increased rates during peak hours may further burden residents during extreme heat events, when indoor cooling may be most needed.

Finally, we note that our study considers a single year (2018) compared to an analog taken from a single year from a GCM end of

century 30-year output. Although our analysis shows geospatial disparities in the cooling energy burden, actual values will vary depending on how cool or warm a particular summer might be. For example, as the energy burden is a function of household income, significantly warmer summers would increase low-income households' burden at higher rates than their higher income counterparts. In addition, limitations related to model resolution could be addressed with increased computing power and finer scale AC adoption rates data, which might improve the representation of spatial characteristics of energy burden.

Nevertheless, our study highlights the disparities spatial distribution of the impacts of current heat exposure across current socioeconomic groups. Our results show that, all things remaining equal, future conditions have the potential to disproportionately affect groups that have fewer means to adapt to these changes. These neighborhoods also stand to experience the highest increases in indoor heat exposure due to a combination of indoor thermal conditions (e.g., occupancy) and outdoor conditions, and our results show increasing risk of heat-related illness and mortality when no adaptations are used. Moreover, by quantifying potential future impacts of future climate on current populations, current policy can focus on strategies to mitigate or avoid them altogether. We also show that, although there are state and local programs to mitigate some of the cost of AC technology (e.g., HEAP), operational costs may pose a significant barrier for their and operation, which might exacerbate negative impacts related to heat exposure under changing climate conditions. Similar studies on the role of socioeconomic factors on exposure and vulnerability to extreme heat (either outdoor or indoor) have been reported across the US in cities like Portland (Voelkel et al. 2018), Chicago (Klinenberg 1999; Wilson and Chakraborty 2019), and San Juan (Méndez-Lázaro et al. 2018), and studies like this might prove useful to reveal what disparities, if any, exist in cooling energy burdens.

Declaration of Competing Interest

The authors declare that they have no known competing financial interests or personal relationships that could have appeared to influence the work reported in this paper.

Acknowledgments

This material is based upon work supported by the NSF-funded Urban Resilience to Extreme Weather-Related Events Sustainability Research Network (UREx SRN; NSF grant #1444755) and NSF grants #1927167 and #1934933. Additional support provided by The National Oceanic and Atmospheric Administration – Cooperative Science Center for Earth System Sciences and Remote Sensing Technologies under the Cooperative Agreement Grant #: NA16SEC4810008. The authors would like to thank The City College of New York, NOAA Center for Earth System Sciences and Remote Sensing Technologies, and NOAA Office of Education, Educational Partnership Program for fellowship support for Harold Gamarro. The statements contained within the manuscript/research article/poster are not the opinions of the funding agency or the US government, but reflect the author's opinions. Computing infrastructure was supported, in part, under National Science Foundation Grants CNS-0958379, CNS-0855217, ACI-1126113 and the City University of New York High Performance Computing Center at the College of Staten Island.

References

Ahmed, K., Ortiz, L. E., & González, J. E. (2017). On the Spatio-Temporal End-User Energy Demands of a Dense Urban Environment. *Journal of Solar Energy Engineering, 139*, Article 041005. https://doi.org/10.1115/1.4036545

American Society of Heating, R. and A.-C. E.. (2017). *2017 ASHRAE handbook: Fundamentals SI edition. ASHRAE*, 2017, ©2017.

Ao, X., Wang, L., Zhi, X., Gu, W., Yang, H., & Li, D. (2019). Observed Synergies between Urban Heat Islands and Heat Waves and Their Controlling Factors in Shanghai, China. *J. Appl. Meteor. Climatol, 58*, 1955–1972. https://doi.org/10.1175/JAMC-D-19-0073.1

ASHRAE. (2017). Standard 55-2017 - Thermal Environmental Conditions for Human Occupancy. *(ANSI/ASHRAE Approved)*. ASHRAE https://www.techstreet.com/ashrae/standards/ashrae-55-2017?product_id=1994974 Accessed September 9, 2019.

Aynsley, R. (2006). Indoor Wind Speed Coefficients for Estimating Summer Comfort. *International Journal of Ventilation, 5*, 3–12. https://doi.org/10.1080/14733315.2006.11683719

Beccali, M., Cellura, M., Brano, V. Lo, & Marvuglia, A. (2004). Forecasting daily urban electric load profiles using artificial neural networks. *Energy Conversion and Management, 45*, 2879–2900. https://doi.org/10.1016/j.enconman.2004.01.006

Bhattacharya, J., DeLeire, T., Haider, S., & Currie, J. (2003). Heat or Eat? Cold-Weather Shocks and Nutrition in Poor American Families. *Am J Public Health, 93*, 1149–1154. https://doi.org/10.2105/AJPH.93.7.1149

Burian, S., & Shepherd, M. (2008). *National building statistics database*. version 2.

Calì, D., Osterhage, T., Streblow, R., & Müller, D. (2016). Energy performance gap in refurbished German dwellings: Lesson learned from a field test. *Energy and Buildings, 127*, 1146–1158. https://doi.org/10.1016/j.enbuild.2016.05.020

Chen, H.-C., Han, Q., & De Vries, B. (2020). Modeling the spatial relation between urban morphology, land surface temperature and urban energy demand. *Sustainable Cities and Society, 60*, Article 102246. https://doi.org/10.1016/j.scs.2020.102246

Chester, M. V., Underwood, B. S., & Samaras, C. (2020). Keeping infrastructure reliable under climate uncertainty. *Nature Climate Change, 10*, 488–490. https://doi.org/10.1038/s41558-020-0741-0

Consolidated Edison, 2021a: About Con Edison's Rates | Con Edison. https://www.coned.com/en/accounts-billing/your-bill/about-con-edisons-rates (Accessed June 2, 2021).

Coumou, D., & Robinson, A. (2013). Historic and future increase in the global land area affected by monthly heat extremes. *Environmental Research Letters, 8*, Article 034018. https://doi.org/10.1088/1748-9326/8/3/034018

Crawley, D. B., & Coauthors. (2001). EnergyPlus: creating a new-generation building energy simulation program. In *Energy and Buildings, 33* pp. 319–331). https://doi.org/10.1016/S0378-7788(00)00114-6

Dimoudi, A., Zoras, S., Kantzioura, A., Stogiannou, X., Kosmopoulos, P., & Pallas, C. (2014). Use of cool materials and other bioclimatic interventions in outdoor places in order to mitigate the urban heat island in a medium size city in Greece. *Sustainable Cities and Society, 13*, 89–96. https://doi.org/10.1016/j.scs.2014.04.003

Energy Information Agency. (2015). *Residential Energy Consumption Survey (RECS) - Data - U.S*. https://www.eia.gov/consumption/residential/data/2015/ (Accessed September 5, 2019).

Farhadi, H., Faizi, M., & Sanaieian, H. (2019). Mitigating the urban heat island in a residential area in Tehran: Investigating the role of vegetation, materials, and orientation of buildings. *Sustainable Cities and Society, 46*, Article 101448. https://doi.org/10.1016/j.scs.2019.101448

Founda, D., & Santamouris, M. (2012). 2017: Synergies between Urban Heat Island and Heat Waves in Athens (Greece), during an extremely hot summer. *Scientific Reports, 7*. https://doi.org/10.1038/s41598-017-11407-6

Gamarro, H., Ortiz, L., & González, J. E. (2020). Adapting to Extreme Heat: Social, Atmospheric, and Infrastructure Impacts of Air-Conditioning in Megacities—The Case of New York City. *ASME Journal of Engineering for Sustainable Buildings and Cities, 1*, Article 031005. https://doi.org/10.1115/1.4048175

Gedzelman, S. D., Austin, S., Cermak, R., Stefano, N., Partridge, S., Quesenberry, S., & Robinson, D. A. (2003). Mesoscale aspects of the urban heat island around New York City. *Theor. Appl. Climatol, 75*, 29–42. https://doi.org/10.1007/s00704-002-0724-2

González, J. E., & Coauthors. (2019). New York City Panel on Climate Change 2019 Report Chapter 2: New Methods for Assessing Extreme Temperatures, Heavy Downpours, and Drought. *Annals of the New York Academy of Sciences, 1439*, 30–70. https://doi.org/10.1111/nyas.14007

González, J., Horton, R., Lin, W., Wu, W., Ramamurthy, P., Arend, M., & Bornstein, R. D. (2019). High-resolution projections of extreme heat in New York City. *International Journal of Climatology, 39*, 4721–4735. https://doi.org/10.1002/joc.6102

Gutiérrez, E., González, J. E., Martilli, A., & Bornstein, R. (2015a). On the anthropogenic heat fluxes using an air conditioning evaporative cooling parameterization for mesoscale urban canopy models. *Journal of Solar Energy Engineering, 137*, Article 051005. https://doi.org/10.1115/1.4030854

Gutiérrez, E., Martilli, A., Santiago, J. L., & González, J. E. (2015b). A Mechanical Drag Coefficient Formulation and Urban Canopy Parameter Assimilation Technique for Complex Urban Environments. *Boundary-Layer Meteorology, 157*, 333–341. https://doi.org/10.1007/s10546-015-0051-7

Hamstead, Z. A., Farmer, C., & McPhearson, T. (2018). Landscape-Based Extreme Heat Vulnerability Assessment. *J. of Extr. Even, 05*, Article 1850018. https://doi.org/10.1142/S2345737618500185

Hills, J. (2012). Getting the measure of fuel poverty: *Final Report of the Fuel Poverty Review*.

Hong, T., Chen, Y., Lee, S. H., & Piette, M. A. (2016). *CityBES: A web-based platform to support city-scale building energy efficiency* (p. 14). Urban Computing.

Hsu, A., Sheriff, G., Chakraborty, T., & Manya, D. (2021). Disproportionate exposure to urban heat island intensity across major US cities. *Nat Commun, 12*. https://doi.org/10.1038/s41467-021-22799-5, 2721.

Iacono, M. J., Delamere, J. S., Mlawer, E. J., Shephard, M. W., Clough, S. A., & Collins, W. D. (2008). Radiative forcing by long-lived greenhouse gases: Calculations with the AER radiative transfer models. *J. Geophys. Res., 113*, D13103. https://doi.org/10.1029/2008JD009944

International Energy Agency. (2018). *The Future of Cooling: Opportunities for energy-efficient air conditioning*. OECD.

Ito, K., Lane, K., & Olson, C. (2018). Equitable Access to Air Conditioning: A City Health Department's Perspective on Preventing Heat-related Deaths. *Epidemiology, 29*, 749–752. https://doi.org/10.1097/EDE.0000000000000912

Jack, D., Anderson, G. B., Bell, M. L., & Kinney, P. L. (2015b). Temperature, ozone, and mortality in urban and non-urban counties in the Northeastern United States. *Environmental Health, 14*, 1–11. https://doi.org/10.1186/1476-069X-14-3

Jaffal, I., Ouldboukhitine, S.-E., & Belarbi, R. (2012). A comprehensive study of the impact of green roofs on building energy performance. *Renewable Energy, 43*, 157–164. https://doi.org/10.1016/j.renene.2011.12.004

Jain, R. K., Smith, K. M., Culligan, P. J., & Taylor, J. E. (2014). Forecasting energy consumption of multi-family residential buildings using support vector regression: Investigating the impact of temporal and spatial monitoring granularity on performance accuracy. *Applied Energy, 123*, 168–178. https://doi.org/10.1016/j.apenergy.2014.02.057

Janjić, Z. I. (1994). The Step-Mountain Eta Coordinate Model: Further Developments of the Convection, Viscous Sublayer, and Turbulence Closure Schemes. *Monthly Weather Review, 122*, 927–945. https://doi.org/10.1175/1520-0493, 1994122<0927:TSMECM>2.0.CO;2.

Kain, J. S. (2004). The Kain–Fritsch convective parameterization: an update. *Journal of Applied Meteorology, 43*, 170–181. https://doi.org/10.1175/1520-0450, 2004043<0170:TKCPAU>2.0.CO;2.

Klinenberg, E. (1999). Denaturalizing disaster: A social autopsy of the 1995 Chicago heat wave. *Theory and Society, 28*, 239–295. https://doi.org/10.1023/A:1006995507723

Knowlton, K., Lynn, B., Goldberg, R. A., Rosenzweig, C., Hogrefe, C., Rosenthal, J. K., & Kinney, P. L. (2007). Projecting Heat-Related Mortality Impacts Under a Changing Climate in the New York City Region. *Am J Public Health, 97*, 2028–2034. https://doi.org/10.2105/AJPH.2006.102947

Kontokosta, C. E., & Tull, C. (2017). A data-driven predictive model of city-scale energy use in buildings. *Applied Energy, 197*, 303–317. https://doi.org/10.1016/j.apenergy.2017.04.005

Lehner, F., Deser, C., & Sanderson, B. M. (2018). Future risk of record-breaking summer temperatures and its mitigation. *Climatic Change, 146*, 363–375. https://doi.org/10.1007/s10584-016-1616-2

Li, D., & Bou-Zeid, E. (2013). Synergistic interactions between urban heat islands and heat waves: The impact in cities is larger than the sum of its parts. *Journal of Applied Meteorology and Climatology, 52*, 2051–2064. https://doi.org/10.1175/JAMC-D-13-02.1

Liao, J., Wang, T., Wang, X., Xie, M., Jiang, Z., Huang, X., & Zhu, J. (2014). Impacts of different urban canopy schemes in WRF/Chem on regional climate and air quality in Yangtze River Delta, China. *Atmospheric Research*, 226–243. https://doi.org/10.1016/j.atmosres.2014.04.005, 145–146.

Limaye, V. S. J., Vargo, M., Harkey, T., Holloway, & J. A, Patz (2018). Climate Change and Heat-Related Excess Mortality in the Eastern USA. *EcoHealth, 15*, 485–496. https://doi.org/10.1007/s10393-018-1363-0

Méndez-Lázaro, P. F. E., Muller-Karger, D., Otis, M. J., McCarthy, & E, Rodríguez (2018). A heat vulnerability index to improve urban public health management in San Juan, Puerto Rico. *Int J Biometeorol, 62*, 709–722. https://doi.org/10.1007/s00484-017-1319-z

Madrigano, J., Ito, K., Johnson, S., Kinney, P. L., & Matte, T. (2015a). A Case-Only Study of Vulnerability to Heat Wave–RelatedMortality in New York City (2000–2011). *Environmental Health Perspectives, 123*, 672–678. https://doi.org/10.1289/ehp.1408178

Martilli, A., Clappier, A., & Rotach, M. W. (2002). An urban surface exchange parameterisation for mesoscale models. *Boundary-Layer Meteorology, 104*, 261–304.

Martilli, A. (2016). Citywide Impacts of Cool Roof and Rooftop Solar Photovoltaic Deployment on Near-Surface Air Temperature and Cooling Energy Demand. *Boundary-Layer Meteorology*. https://doi.org/10.1007/s10546-016-0160-y

Masson, V. (2000). A Physically-Based Scheme For The Urban Energy Budget In Atmospheric Models. *Boundary-Layer Meteorology, 94*, 357–397. https://doi.org/10.1023/A:1002463829265

Meehl, G. A., & Tebaldi, C. (2004). More intense, more frequent, and longer lasting heat waves in the 21st century. *Science, 305*, 994–997. https://doi.org/10.1126/science.1098704

Mesinger, F., & Coauthors. (2006). North American Regional Reanalysis. *Bulletin of the American Meteorological Society, 87*, 343–360. https://doi.org/10.1175/BAMS-87-3-343

Mlawer, E. J., Taubman, S. J., Brown, P. D., Iacono, M. J., & Clough, S. A. (1997). Radiative transfer for inhomogeneous atmospheres: RRTM, a validated correlated-k model for the longwave. *Journal of Geophysical Research, 102*, 16663. https://doi.org/10.1029/97JD00237

Monaghan, A. J., Steinhoff, D. F., Bruyere, C. L., & Yates, D. (2014). *NCAR CESM Global Bias-Corrected CMIP5 Output to Support WRF/MPAS Research*. https://doi.org/10.5065/D6DJ5CN4

Mughal, M. O., Li, X.-X., & Norford, L. K. (2020). Urban heat island mitigation in Singapore: Evaluation using WRF/multilayer urban canopy model and local climate zones. *Urban Climate, 34*, Article 100714. https://doi.org/10.1016/j.uclim.2020.100714

Neto, A. H., & Fiorelli, F. A. S. (2008). Comparison between detailed model simulation and artificial neural network for forecasting building energy consumption. *Energy and Buildings, 40*, 2169–2176. https://doi.org/10.1016/j.enbuild.2008.06.013

New York City Office of the Mayor. (2017). *New York City Government Poverty Measure 2017*.

Oke, T. R. (1982). The energetic basis of the urban heat island. *Quarterly Journal of the Royal Meteorological Society, 108*, 1–24. https://doi.org/10.1002/qj.49710845502

Olivo, Y., Hamidi, A., & Ramamurthy, P. (2017). Spatiotemporal variability in building energy use in New York City. *Energy, 141*, 1393–1401. https://doi.org/10.1016/j.energy.2017.11.066

Ortiz, L., González, J. E., & Lin, W. (2018a). Climate change impacts on peak building cooling energy demand in a coastal megacity. *Environmental Research Letters, 13*, Article 094008. https://doi.org/10.1088/1748-9326/aad8d0

Ortiz, L. E., Gonzalez, J. E., Gutierrez, E., & Arend, M. (2016). Forecasting Building Energy Demands With a Coupled Weather-Building Energy Model in a Dense Urban Environment. *Journal of Solar Energy Engineering, 139*, Article 011002. https://doi.org/10.1115/1.4034909

Palma, P., Gouveia, J. P., & Simoes, S. G. (2019). Mapping the energy performance gap of dwelling stock at high-resolution scale: Implications for thermal comfort in Portuguese households. *Energy and Buildings, 190*, 246–261. https://doi.org/10.1016/j.enbuild.2019.03.002

Pokhrel, R., Ramírez-Beltran, N. D., & González, J. E. (2018). On the assessment of alternatives for building cooling load reductions for a tropical coastal city. *Energy and Buildings*. https://doi.org/10.1016/j.enbuild.2018.10.023

Quinn, A., Tamerius, J. D., Perzanowski, M., Jacobson, J. S., Goldstein, I., Acosta, L., & Shaman, J. (2014). Predicting indoor heat exposure risk during extreme heat events. *Science of The Total Environment, 490*, 686–693. https://doi.org/10.1016/j.scitotenv.2014.05.039

Quinn, A., Kinney, P., & Shaman, J. (2017). Predictors of summertime heat index levels in New York City apartments. *Indoor Air, 27*, 840–851. https://doi.org/10.1111/ina.12367

Rahmstorf, S. (2013). Global increase in record-breaking monthly-mean temperatures. *Climatic Change, 118*, 771–782. https://doi.org/10.1007/s10584-012-0668-1

Ramamurthy, P., González, J., Ortiz, L., Arend, M., & Moshary, F. (2017). Impact of heatwave on a megacity: an observational analysis of New York City during July 2016. *Environmental Research Letters, 12*, Article 054011. https://doi.org/10.1088/1748-9326/aa6e59

Roberts, S. (2008). Energy, equity and the future of the fuel poor. *Energy Policy, 36*, 4471–4474. https://doi.org/10.1016/j.enpol.2008.09.025

Robinson, C., Bouzarovski, S., & Lindley, S. (2018). Getting the measure of fuel poverty': The geography of fuel poverty indicators in England. *Energy Research & Social Science, 36*, 79–93. https://doi.org/10.1016/j.erss.2017.09.035

Rosenthal, J., Kinney, P. L., & Metzger, K. B. (2014). Intra-urban vulnerability to heat-related mortality in New York City, 1997–2006. *Health & Place, 30*, 45–60. https://doi.org/10.1016/j.healthplace.2014.07.014

Rothfusz, L. P. (1990). *The heat index equation (or, more than you ever wanted to know about heat index)*. NWS Southern Region Headquarters.

Salamanca, F., Krpo, A., Martilli, A., & Clappier, A. (2010). A new building energy model coupled with an urban canopy parameterization for urban climate simulations—Part I. Formulation, verification, and sensitivity analysis of the model. *Theoretical and Applied Climatology, 99*, 331–344. https://doi.org/10.1007/s00704-009-0142-9

Salamanca, F., Georgescu, M., Mahalov, A., Moustaoui, M., Wang, M., & Svoma, B. M. (2013). Assessing summertime urban air conditioning consumption in a semiarid environment. *Environmental Research Letters, 8*, Article 034022. https://doi.org/10.1088/1748-9326/8/3/034022

Salamanca, F., Georgescu, M., Mahalov, A., & Moustaoui, M. (2015). Summertime Response of Temperature and Cooling Energy Demand to Urban Expansion in a Semiarid Environment. *Journal of Applied Meteorology and Climatology, 54*, 1756–1772. https://doi.org/10.1175/JAMC-D-14-0313.1

Santamouris, M. (2016). Cooling the buildings – past, present and future. *Energy and Buildings, 128*, 617–638. https://doi.org/10.1016/j.enbuild.2016.07.034

Santiago, J. L., Coceal, O., Martilli, A., & Belcher, S. E. (2008). Variation of the Sectional Drag Coefficient of a Group of Buildings with Packing Density. *Boundary-Layer Meteorology, 128*, 445–457. https://doi.org/10.1007/s10546-008-9294-x

Schmidt, K., & Patterson, D. J. (2001). Performance results for a high efficiency tropical ceiling fan and comparisons with conventional fans. *Renewable Energy, 22*, 169–176. https://doi.org/10.1016/S0960-1481(00)00056-2

Short, T., & Swayne, T. (2012). *Assessment of transmission and distribution losses in New York State*. EPRI.

Skamarock, W., Klemp, J., Dudhia, J., Gill, D., Barker, D., Wang, W., Huang, X., & Duda, M. (2008). *A description of the Advanced Research WRF version 3*. https://doi.org/10.5065/D68S4MVH

Skelhorn, C. P., Levermore, G., & Lindley, S. J. (2016). Impacts on cooling energy consumption due to the UHI and vegetation changes in Manchester, UK. *Energy and Buildings, 122*, 150–159. https://doi.org/10.1016/j.enbuild.2016.01.035

Steadman, R. G. (1979). The Assessment of Sultriness. Part I: A Temperature-Humidity Index Based on Human Physiology and Clothing Science. *J. Appl. Meteor., 18*, 861–873. https://doi.org/10.1175/1520-0450, 1979018<0861:TAOSPI>2.0.CO;2.

Sunikka-Blank, M., & Galvin, R. (2012). Introducing the prebound effect: the gap between performance and actual energy consumption. *Building Research & Information, 40*, 260–273. https://doi.org/10.1080/09613218.2012.690952

Teller-Elsberg, J., Sovacool, B., Smith, T., & Laine, E. (2016). Fuel poverty, excess winter deaths, and energy costs in Vermont: Burdensome for whom? *Energy Policy, 90*, 81–91. https://doi.org/10.1016/j.enpol.2015.12.009

Tewari, M., & Coauthors. (2004). Implementation and verification of the unified NOAH land surface model in the WRF model. 20th conference on weather analysis and forecasting/16th conference on numerical weather prediction. *Seattle*, 11–15. WA.

Thompson, G., Field, P. R., Rasmussen, R. M., & Hall, W. D. (2008). Explicit Forecasts of Winter Precipitation Using an Improved Bulk Microphysics Scheme. Part II: Implementation of a New Snow Parameterization. *Mon. Wea. Rev., 136*, 5095–5115. https://doi.org/10.1175/2008MWR2387.1

Time-Of-Use Rates, Con Edison. 2021b https://www.coned.com/en/accounts-billing/your-bill/time-of-use (Accessed June 2, 2021).

Tsilini, V., Papantoniou, S., Kolokotsa, D.-D., & Maria, E.-A. (2015). Urban gardens as a solution to energy poverty and urban heat island. *Sustainable Cities and Society, 14*, 323–333. https://doi.org/10.1016/j.scs.2014.08.006

U. S. Census Bureau. (2019). *American Community Survey, 2018 American Community Survey 1-Year Estimates*.

Uejio, C. K., Tamerius, J. D., Vredenburg, J., Asaeda, G., Isaacs, D. A., Braun, J., Quinn, A., & Freese, J. P. (2016). Summer indoor heat exposure and respiratory and cardiovascular distress calls in New York City, NY, U.S. *Indoor Air, 26*, 594–604. https://doi.org/10.1111/ina.12227

United Nations. (2019). *World population prospects Highlights, 2019 revision Highlights, 2019 revision*.

van Loenhout, J. A. F., le Grand, A., Duijm, F., Greven, F., Vink, N. M., Hoek, G., & Zuurbier, M. (2016). The effect of high indoor temperatures on self-perceived health of elderly persons. *Environmental Research, 146*, 27–34. https://doi.org/10.1016/j.envres.2015.12.012

Vant-Hull, B., & Coauthors. (2018). The Harlem Heat Project: A Unique Media–Community Collaboration to Study Indoor Heat Waves. *Bull. Amer. Meteor. Soc., 99*, 2491–2506. https://doi.org/10.1175/BAMS-D-16-0280.1

Viguie, V., Lemonsu, A., Hallegatte, S., Beaulant, A.-L., Marchadier, C., Masson, V., Pigeon, G., & Salagnac, J.-L. (2020). Early adaptation to heat waves and future reduction of air-conditioning energy use in Paris. *Environ. Res. Lett.*. https://doi.org/10.1088/1748-9326/ab6a24

Voelkel, J., Hellman, D., Sakuma, R., & Shandas, V. (2018). Assessing Vulnerability to Urban Heat: A Study of Disproportionate Heat Exposure and Access to Refuge by Socio-Demographic Status in Portland, Oregon. *International Journal of Environmental Research and Public Health, 15*(640). https://doi.org/10.3390/ijerph15040640

Waite, M., Cohen, E., Torbey, H., Piccirilli, M., Tian, Y., & Modi, V. (2017). Global trends in urban electricity demands for cooling and heating. *Energy*. https://doi.org/10.1016/j.energy.2017.03.095

Wang, H., & Chen, Q. (2014). Impact of climate change heating and cooling energy use in buildings in the United States. *Energy and Buildings, 82*, 428–436. https://doi.org/10.1016/j.enbuild.2014.07.034

Wilson, B., & Chakraborty, A. (2019). Mapping vulnerability to extreme heat events: lessons from metropolitan Chicago. *Journal of Environmental Planning and Management, 62*, 1065–1088. https://doi.org/10.1080/09640568.2018.1462475

Xu, X., Chen, F., Shen, S., Miao, S., Barlage, M., Guo, W., & Mahalov, A. (2018). Using WRF-Urban to Assess Summertime Air Conditioning Electric Loads and Their Impacts on Urban Weather in Beijing. *Journal of Geophysical Research: Atmospheres*. https://doi.org/10.1002/2017JD028168

Yan, L., & Liu, M. (2020). A simplified prediction model for energy use of air conditioner in residential buildings based on monitoring data from the cloud platform. *Sustainable Cities and Society, 60*, Article 102194. https://doi.org/10.1016/j.scs.2020.102194